

# LiveHand: Real-time and Photorealistic Neural Hand Rendering

AKSHAY MUNDRA, Max Planck Institute for Informatics and Saarland University

MALLIKARJUN B R, Max Planck Institute for Informatics

JIAYI WANG, Max Planck Institute for Informatics

MARC HABERMANN, Max Planck Institute for Informatics

CHRISTIAN THEOBALT, Max Planck Institute for Informatics and Saarland University

MOHAMED ELGHARIB, Max Planck Institute for Informatics

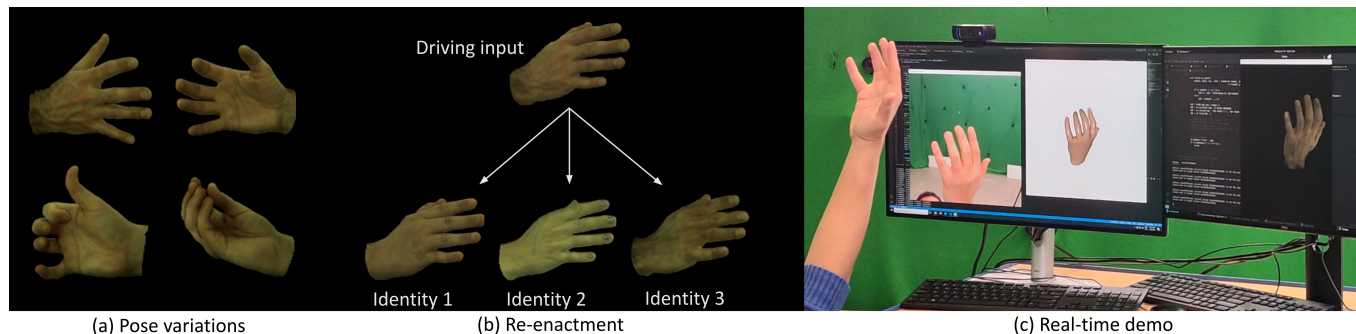


Fig. 1. We present LiveHand, the first neural implicit approach for rendering articulated hands in real-time. (a) Our method captures pose-dependent effects such as hand shadows, popping veins, and skin wrinkles. (b) We can use the hand-pose obtained from an input sequence to re-enact different identities. (c) Our method is designed for optimal rendering speed and quality – we show a live demo where we track the 3D hand-pose and render a photo-realistic hand avatar, all in real-time.

The human hand is the main medium through which we interact with our surroundings, making its digitization an important problem. Hence, its digitization is of uttermost importance, with direct applications in VR/AR, gaming, and media production amongst other areas. While there are several works modeling the geometry of hands, little attention has been paid to capturing photo-realistic appearance. Moreover, for applications in extended reality and gaming, real-time rendering is critical. We present the first neural-implicit approach to photo-realistically render hands in real-time. This is a challenging problem as hands are textured and undergo strong articulations with pose-dependent effects. However, we show that this aim is achievable through our carefully designed method. This includes training on a low-resolution rendering of a neural radiance field, together with a 3D-consistent super-resolution module and mesh-guided sampling and space canonicalization. We demonstrate a novel application of perceptual loss on the image space, which is critical for learning details accurately. We also show a live demo where we photo-realistically render the human hand in real-time for the first time, while also modeling pose- and view-dependent appearance effects. We ablate all our design choices and show that they optimize for rendering speed and quality. Our code will be released to encourage further research in this area.

Additional Key Words and Phrases: Human digitalization, neural rendering, hand modeling

## 1 INTRODUCTION

As the popularity of VR/AR technology rises, providing a natural interface with these digital contents becomes vital. Without a doubt, hands are the most intuitive mode of interaction for users in a 3D environment. Therefore, it is quintessential to digitize the users' hands to render their personalized, controllable, and photorealistic

counterparts in the virtual world. Achieving this is a challenging task since hand appearance is a complex function that varies with both pose and viewing direction. Moreover, ensuring the real-time performance of such a system is key to enabling applications such as telepresence, teleoperation, and computer-aided design.

While the creation of photorealistic hand models is possible to some extent using traditional computer graphics techniques, it typically requires extensive manual efforts from experienced artists. Therefore, recent research has started to investigate whether hand models can be directly derived from 2D imagery. Here, most existing methods use some data-driven explicit model to constrain the hand geometry and appearance to a low dimensional space for the sake of tractability and robustness to occlusions [Li et al. 2021, 2022; Moon et al. 2020a; Qian et al. 2020; Romero et al. 2017]. Reconstruction is then formulated as a search in this space for the best-fitting parameters. Although these approaches can rapidly provide plausible results, the reconstruction is constrained to the space spanned by the registered hand mesh data used to create the model, thus limiting the visual quality and level of personalization.

More recently, neural implicit representations [Mildenhall et al. 2020] have shown impressive results on static scenes for novel-view synthesis. Some works have extended these formulations beyond static scenes to enable photorealistic renderings of articulated objects such as the human body [Habermann et al. 2022, 2021; Liu et al. 2021; Noguchi et al. 2021; Peng et al. 2021a,b; Su et al. 2021; Yang et al. 2022]. Despite their successes, very little work has been done applying these ideas to hands. In contrast to bodies, hand motions exhibit more severe self-occlusions and more self-contact, which

hinders the learning of scene representations that are consistent across different articulations. One particular work of interest is LISA [Corona et al. 2022], which proposed a method to create neural hand avatars. Although their approach shows promising results, it does not support real-time rendering during inference and the results lack high-frequency details.

In this paper, we propose the first method for creating a *photo-realistic* neural hand avatar, which achieves *real-time* performance while being solely learned from segmented multi-view video of an articulated hand and respective hand pose annotations (see Fig. 1). To this end, we introduce a hybrid hand model representation using the MANO hand model as a coarse proxy, which is surrounded by a neural radiance field. The idea is to simplify the learning problem by bounding the learnable volume through the canonicalization of global coordinates into a texture cube. These normalized coordinates can then be fed into a shallow coordinate-based MLP to regress the scene color and density. This formulation can also leverage the coarse mesh proxy for more efficient sampling of a low-resolution NeRF representation of the scene; we show that this, when combined with a CNN-based super-resolution module carefully designed for efficient upsampling, can achieve real-time performance. Moreover, we found that our highly efficient representation allows training not only on a few ray samples per iteration but on full images. Therefore, we can for the first time supervise an implicit scene representation using a perceptual loss on *full images* during training. Again our experiments show that this greatly improves our results over the baseline, which runs perceptual supervision on a patch basis. Together, these design choices allow us to render and re-enact photo-realistic hands in real-time detailed enough to capture even pose- and view-dependent appearance changes. In summary, our contributions are:

- We propose LiveHand, the first method for real-time photorealistic neural hand rendering.
- The real-time performance is achieved with our careful combination of design choices, namely, a mesh-guided 3D sampling strategy, a low-resolution neural radiance field, and a 3D-consistent super-resolution module.
- With these computationally-efficient design choices, we for the first time demonstrate that a perceptual loss on the full image can be effectively used for supervising implicit representations and that it outperforms the commonly used patch-based loss.

Our results demonstrate that we outperform the state of the art in terms of visual quality and runtime performance. Moreover, we show a live demo of our approach, which convincingly shows the straightforward use of our method in daily life scenarios. We will release our code and data for future research.

## 2 RELATED WORKS

**Geometry Modeling.** Parametric 3D morphable models map low-dimensional control variables to deforming meshes enabling easy and efficient control of the generated geometry [Alldieck et al. 2021; Li et al. 2017; Pavlakos et al. 2019; Romero et al. 2017]. Relevant to our work, MANO [Romero et al. 2017] learns a parametric hand model using high-resolution 3D scans, parametrizing the mesh as a

Table 1. **Conceptual comparison of our method with other hand-modeling approaches.**

Methods	Real-time	Photo-real	Pose-dep. app.	View-dep. app.
HTML [Qian et al. 2020]	✓	✗	✗	✗
NIMBLE [Li et al. 2022]	✓	✓	✗	✗
LISA [Corona et al. 2022]	✗	✗	✓	✗
<b>Ours</b>	✓	✓	✓	✓

function of the hand shape and pose. Implicit geometry modeling uses a neural network to encode the geometry as an isosurface. Since the learned representation is resolution-independent, it can - in theory - be used to retrieve meshes at arbitrarily-high resolution at inference time. imGHUM [Alldieck et al. 2021] builds a parametric full-body model comprising of detailed body, face, and hand geometry. GraspingField [Karunratanakul et al. 2020] learns a signed distance function (SDF) of hand-object interaction, which fits the MANO model onto the SDF to recover the final pose estimate. However, none of the existing works [Karunratanakul et al. 2021, 2020; Li et al. 2021; Moon et al. 2020a; Romero et al. 2017] include a component for the hand texture. In contrast, our goal is to model the photorealistic hand appearance in real-time.

**Geometry and Appearance Modeling.** A few approaches extend parametric mesh by complementing it with a texture map. HTML [Qian et al. 2020] builds a low-dimensional hand appearance model by applying principal component analysis (PCA) to texture maps of 51 subjects. NIMBLE [Li et al. 2022] uses MRI data to learn a parametric mesh model based on the bones and muscles, and uses light-stage captures to obtain the appearance maps (including albedo, normal maps, and specular maps). A PCA on the various components of appearance maps give them an appearance model. Since both HTML and NIMBLE use a linear model to compress the appearance variations to a low-dimensional space, their expressivity is severely limited. For example, they lack details such as veins and colored fingernails since these are person-specific attributes. Closest to our approach is LISA [Corona et al. 2022], which models the hand shape and appearance using a neural implicit field. The underlying MLPs are conditioned on pose and appearance parameters, allowing pose and appearance changes at inference. However, the reconstructions lack high-frequency details, and the approach takes about one minute to render an image at  $1024 \times 667$  pixels. On the other hand, we focus on creating a digital hand avatar in a person-specific setup and show photorealistic results in real-time. Please refer to Tab. 1 for a conceptual comparison of the existing hand modeling methods.

**Other Animatable Objects.** The literature contains works for modeling other animatable objects such as the human face [Cao et al. 2022; Gao et al. 2022; Grassal et al. 2022; Lombardi et al. 2021; Zheng et al. 2022], human body [Bhatnagar et al. 2020; Habermann et al. 2021; Liu et al. 2021; Peng et al. 2021b; Su et al. 2021; Xu et al. 2011; Yang et al. 2022], and animals [Luo et al. 2022]. The face related methods can not handle large deformations [Cao et al. 2022; Gao et al. 2022; Lombardi et al. 2021] and/or are not real-time [Gao et al. 2022; Grassal et al. 2022; Zheng et al. 2022], while [Luo et al. 2022] does not model pose-dependent appearance effects. To handle

more articulated motions that occur in the human body, two classes of body-specific methods have been proposed. The explicit mesh-based methods [Bagautdinov et al. 2021; Habermann et al. 2021; Ma et al. 2021; Xu et al. 2011] rely on a template mesh obtained from a static scene and then learn appearance in the mesh space. However, due to the strong reliance on a template mesh, the learned appearance becomes blurry if the deformed template mesh does not match the real deformation of the surface. Other mesh-based approaches [Prokudin et al. 2021; Raj et al. 2021] do not model pose or view-dependent effects. In contrast, neural implicit models can learn more fine-grained deformations at much higher resolution. For example, it has been used to model the geometry and appearance of clothed humans [Habermann et al. 2022; Hu et al. 2021; Jiang et al. 2022; Liu et al. 2021; Noguchi et al. 2021; Peng et al. 2021a,b; Su et al. 2021; Yang et al. 2022]. However, these can not operate in real-time. Another line of implicit body-modeling approaches [Remelli et al. 2022; Shao et al. 2022; Suo et al. 2021] require RGB images from multiple cameras at test time, and thus can not be controlled with arbitrary poses. Extending the body modeling methods to human hands is not trivial, as hands exhibit even stronger articulation, which in turn results in severe self-occlusion and other pose-dependent effects. Our proposed method tackles this setting by utilizing elements from both mesh-based and neural implicit modeling to create a detailed model that runs in real-time.

### 3 METHODOLOGY

Given multi-view images  $\{G_j^p | j = 1 \dots N, p = 1 \dots P\}$  for  $P$  frames captured from  $N$  viewpoints and coarse estimates of the corresponding posed parametric hand mesh  $\{\mathcal{M}(\psi^p) | p = 1 \dots P\}$ , our method creates a photo-realistic hand avatar that can accurately model hand-pose and view-dependent appearance effects, and can be rendered in real-time. An overview of our method is shown in Fig. 2. Given the hand parameters  $\psi$ , we can canonicalize every point in the scene based on the point’s projection onto the posed mesh  $\mathcal{M}(\psi)$ . The point coordinates are then re-parameterized in terms of the corresponding texture coordinates after projection. A multi-layer perception (MLP)  $H_\alpha$  is then trained to map the re-parameterized coordinates to a radiance field, conditioned on articulation parameters. For the given camera extrinsics and intrinsics, we render low-resolution images and feature maps using volumetric rendering, which is then up-sampled using a super-resolution network  $S_\phi$  to obtain the final rendering. In this section, we initially describe the hand model required to build the neural hand representation in Sec. 3.1, the scene representation in Sec. 3.2, and its efficient 2D rendering in Sec. 3.3. Finally, in Sec. 3.4, we describe how our neural hand model can be effectively trained.

#### 3.1 MANO Model

We leverage the MANO [Romero et al. 2017] model to parameterize the approximate hand geometry. MANO maps the model parameter  $\psi$  to a posed mesh  $\mathcal{M}$  using its Linear Blend Skinning (LBS) weights  $W$  and a canonical hand mesh  $\overline{\mathcal{M}}$ .

$$\mathcal{M}(\psi) = \text{MANO}(\overline{\mathcal{M}}, \psi, W) \quad (1)$$

$\psi : \{\theta, \beta, t, R\} \in \mathbb{R}^{61}$  consists of the articulation parameters  $\theta \in \mathbb{R}^{45}$ , shape parameters  $\beta \in \mathbb{R}^{10}$ , and the global translation  $t \in \mathbb{R}^3$

and rotation in axis-angle format  $R \in \mathbb{R}^3$ . We refer the readers to [Romero et al. 2017] for more details. For convenience, we also define hand pose as  $\xi : \{\theta, R\} \in \mathbb{R}^{48}$  here.  $\xi$  encodes only the articulation and orientation of the hand, and is, thus, independent of identity and position in global 3D space.

#### 3.2 Implicit Hand Representation

Inspired by the state-of-the-art implicit novel view synthesis method, NeRF [Mildenhall et al. 2020], we model our hand avatar with a view-dependent implicit representation. Since NeRF can only capture static scenes, we must extend the radiance field to account for deformations. In this section, we systematically motivate and describe our chosen representation.

**Naive Conditioning.** One way to formulate the hand radiance field  $H_\alpha$  is by naively conditioning it as follows:

$$H_\alpha : (x, d, \xi) \rightarrow (c, \sigma) \quad (2)$$

where,  $x$  is a point in 3D space,  $d$  is the viewing direction,  $\xi$  is the hand pose,  $c$  is the color and  $\sigma$  is the density. The trainable radiance field  $H_\alpha$  is parameterized by an MLP with parameters  $\alpha$ . However, this leads to poor generalization to novel test hand poses as will be shown in Sec. 4. This is because any point on the hand surface gets mapped to completely different world coordinates based on the hand pose.

**Per-bone Canonicalization.** One way to overcome this problem in the literature [Corona et al. 2022] is to canonicalize the scene with respect to the hand pose. Specifically, a point in world space is transformed into each bone’s local coordinate systems obtained from a skeleton pose estimate. Separate implicit fields are learnt in the local coordinate systems, which are combined as follows:

$$\sigma = \sum_{k=1}^{n_b} w_k \sigma_k, \quad c = \sum_{k=1}^{n_b} w_k c_k \quad (3)$$

where  $w$  is analogous to LBS weights. We evaluate such a canonicalization approach in Sec. 4. Such a per-bone canonicalization requires inferring multiple MLPs for each 3D point, making it slower for both training and inference.

**Mesh-based Canonicalization.** For a more efficient representation, we take inspiration from mesh-based texturing which associates each point on the mesh surface with a 2D texture coordinate  $(u, v) \in [0, 1] \times [0, 1]$  from which a color value can be obtained using a texture image. We extend this surface representation to 3D volumes by introducing a signed distance  $h$  to support volume rendering and to account for the coarseness of the MANO-based geometry approximation. More concretely, for a given point  $x$  in 3D, we first find its projection on the given MANO surface. The  $(u, v)$  co-ordinate of this projected point can be estimated by performing barycentric interpolation on the  $(u, v)$  coordinates of the corresponding mesh-triangle vertices. The signed distance  $h$  of the sampling point to its projection on the mesh is used to disambiguate points orthogonal to the mesh surface [Liu et al. 2021]. With this canonicalization, we can formulate the radiance field mapping as,

$$H_\alpha : (u, v, h, d) \rightarrow (c, \sigma) \quad (4)$$

This allows us to canonicalize the world coordinates to a representation that stays consistent with respect to hand surface irrespective

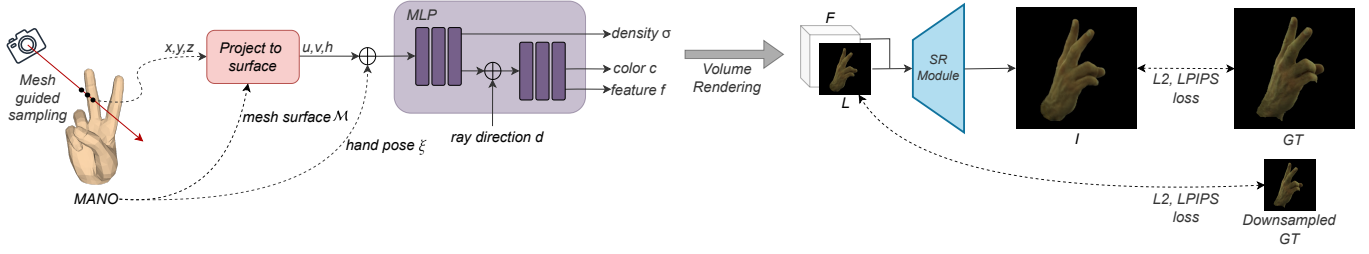


Fig. 2. **Overview of our approach.** Given a hand pose and camera view, our method renders a photorealistic image of the hand in real-time. To this end, we introduce a mesh-based canonicalization that transforms the global points into a texture space. The hand appearance is captured by an MLP that maps points from this texture space to radiance values. We then leverage volume rendering to obtain a low-resolution image-aligned feature tensor where the first three channels contain the RGB image of the hand. Finally, a super-resolution module up-samples the tensor to obtain the final full-resolution image. Since our method achieves very fast inference speeds, we can supervise it with a perceptual loss on the full image resolution.

of hand pose  $\xi$ , thus preventing the dispersion of learned features in the input space. In practice, we apply positional encoding [Mildenhall et al. 2020] to all inputs described in Eq. 4.

Although Eq. 4 is implicitly a function of  $\xi$  due to the dependency of  $(u, v, h)$  on the posed mesh, we find that explicit pose conditioning  $\xi$  is still needed to capture pose-dependent appearance changes. This leads to the modified representation:

$$H_\alpha : (u, v, h, d, \xi) \rightarrow (c, \sigma) \quad (5)$$

Note that although we rely on the coarse hand mesh for canonicalization, the implicit representation  $H_\alpha$  can learn fine-scale details that are hard to model using MANO mesh alone. We show this later in Sec. 4 where our method significantly outperforms a baseline that naively textures the coarse MANO mesh using ground truth images.

### 3.3 Efficient Rendering

Since  $H_\alpha$  is parameterized with an MLP, it can be queried to regress the density  $\sigma$  and color  $c$  for each point in 3D space. For a ray with origin  $\mathbf{o}$  and direction  $\mathbf{d}$ , volumetric integration - as proposed in NeRF [Mildenhall et al. 2020] - can be used to obtain the integrated color  $\mathbf{C}$  for the ray  $\mathbf{r}(t) = \mathbf{o} + t\mathbf{d}$ , with near and far bounds  $t_n$  and  $t_f$  as follow:

$$\mathbf{C}(\mathbf{r}) = \int_{t_n}^{t_f} T(t) \sigma(\mathbf{r}(t)) c(\mathbf{r}(t)) dt$$

where  $T(t) = \exp(-\int_{t_n}^t \sigma(\mathbf{r}(s)) ds)$ . (6)

This integral can be approximated through stratified sampling within the bounds. However, such a strategy will waste samples on regions that do not contain useful features. Hierarchical sampling was introduced in NeRF [Mildenhall et al. 2020] to address this inefficiency. However, this involves the use of two MLPs to encode both the coarse and detailed scene, and sampling the scene twice.

**Mesh-Guided Sampling.** To make the rendering faster, we utilize the coarse MANO geometry to efficiently sample points around the approximate hand surface. Specifically, to define the bounds of each ray, we use the depth rendering of the coarse mesh to constrain the samples to lie close to the approximate surface [Habermann et al.

2022]. This eliminates the two-pass approach needed for hierarchical sampling.

**Super-resolution.** Although this efficient sampling strategy improves the run-time, it still can not achieve real-time rendering speeds. We introduce a super-resolution network [Chan et al. 2022]  $S_\phi$  that can super-resolve the rendered output in a 3D consistent manner. To do so, we first modify the  $H_\alpha$  to additionally predict a 29-channel  $\mathbf{f}$ , which encodes scene features alongside the color to capture additional details. We accomplish this by extending Eq. 4 with:

$$H_\alpha : (u, v, h, d, \xi) \rightarrow (c, \mathbf{f}, \sigma) \quad (7)$$

We then apply volumetric integration as done in Eq. 6 to obtain low-resolution renderings of color  $L_j^p$  and features  $F_j^p$  for each viewpoint  $j$  and hand pose  $p$ . These low-resolution encodings are used in a super-resolution module

$$S_\phi : (L, F) \rightarrow I \quad (8)$$

to recover a high-resolution image  $I_j^p$  that preserves the details. To ensure efficiency, we parameterize  $S_\phi$  using a CNN-based network with the trainable parameters  $\phi$ .

### 3.4 Training

As described in the previous section, we need to learn the parameters of the MLP  $H_\alpha$  and super-resolution module  $S_\phi$  using the multi-view image sequence.

**Color Calibration.** As most multi-view images in general are not color corrected to be consistent across views, we compensate for this, as done in Neural Volumes [Lombardi et al. 2019], by learning separate per-camera gain and bias parameters  $g_j$  and  $b_j$ .

**Objective Function.** We train the parameters of our modules  $H_\alpha$  and  $S_\phi$  in a supervised manner using the following loss functions

$$\mathcal{L} = \mathcal{L}_{rec} + \mathcal{L}_{perc} \quad (9)$$

between ground truth target image  $G_j^p$  and rendering image  $I_j^p$  using gradient descent. Here  $\mathcal{L}_{rec}$  is the L2 reconstruction loss given by:

$$\mathcal{L}_{rec} = \|G_j^p - I_j^p(\alpha, \phi)\|_2 \quad (10)$$



To capture the perceptual difference in the image, we apply  $\mathcal{L}_{perc}$  as suggested in [Zhang et al. 2018]

$$\mathcal{L}_{perc} = \|f(G_j^p) - f(I_j^p(\alpha, \phi))\|_2 \quad (11)$$

Where  $f(\cdot)$  is the activation of the *conv1-conv5* layers in pre-trained VGG network [Simonyan and Zisserman 2014]. Thanks to our efficient design choices, we can apply the perceptual loss on the full image, as opposed to the traditional approach of applying it on smaller patches [Weng et al. 2022]. We show later that the perceptual loss plays a vital role in recovering high-frequency details, and our image-based approach improves photorealism over using the patch-based strategy (see Tab. 4 and Fig. 8). We employ the above loss functions to both low-resolution volumetrically rendered images and super-resolved high-resolution images.

### 3.5 Implementational Details

We use the same positional encoder as [Mildenhall et al. 2020], with a maximum frequency of  $L = 10$  for the canonicalized sampling point  $(u, v, h)$  and  $L = 4$  for the viewing direction  $d$ . Our network is parameterized with a 6 layer-deep MLP as shown in Fig. 3. We use a similar CNN network architecture as in EG3D [Chan et al. 2022] for our super-resolution network, with an upsampling factor of 2. We empirically choose 16 as the number of samples to draw per ray as it best trades off image quality and rendering speed. Our radiance field module  $H_\alpha$ , super-resolution module  $S_\phi$ , and color calibration parameters  $g_j, b_j$  are learnt with learning rates of 0.0025, 0.0025, and 0.0001 respectively using Adam optimizer [Kingma and Ba 2015] with a decay rate of 0.1. All models are trained for 200K iterations.

## 4 EXPERIMENTS

We use the publicly released version of the InterHand2.6M benchmark for our experiments. The dataset contains multi-view sequences of different users performing a wide range of actions at 5fps and  $512 \times 334$  pixels resolution. To test our method, we select the right-hand sequences from four users in the "train/capture0", "train/capture5", "test/capture0", and "test/capture1" subsets. We reserve the last 50 frames of each capture for evaluation and use the rest for training.

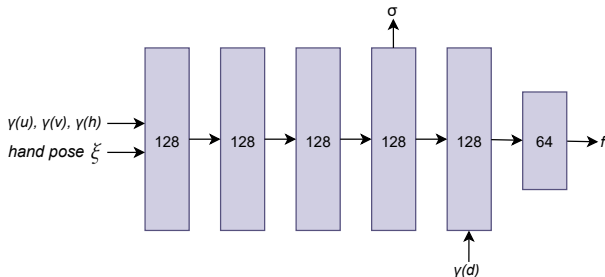


Fig. 3. **MLP architecture of our model.** The uvh mapping simplifies learning the radiance field, allowing us to reduce the network size compared to [Mildenhall et al. 2020].

We show that the advantages of our proposed model work synergistically together to enable the first demo for real-time photo-realistic neural hand reenactment. The details of this demo and its results are presented in Section 4.1. We additionally provide quantitative and qualitative evaluations of our method on the established benchmark in Section 4.2 and Section 4.3. For this, we used PSNR, LPIPS, and FID metrics for numerical evaluation. Following the conventions of [Zhang et al. 2018], LPIPS score is calculated using AlexNet backbone. For rendering speed, we report the time it takes to render an image on an NVIDIA GeForce RTX 3090 at the training resolution (i.e.  $512 \times 334$  pixels) in frames per second (FPS). For super-resolution experiments, volumetric integration produce a rendering at  $256 \times 167$  pixels which are then super-resolved to  $512 \times 334$  pixels. Results show that our method outperforms existing state-of-the-art methods by a large margin and that each component is necessary to achieve this result.

### 4.1 Application: Real-time Hand Reenactment

We carefully design our method specifically for real-time hand reenactment applications. After training our neural implicit representation  $H_\alpha$  and the super-resolution module  $S_\phi$  to create a user's hand avatar, we can drive the articulation of that hand using new motion. Fig. 4 show this transfer of hand performance from a reference user ('Reference') to 4 learned identities. Note that our approach can generalize well across identities even when the driving poses were not seen during training. Note how the avatar of each identity captures high-frequency skin texture as well as hand-pose dependent illumination, which contributes to the photo-realism of our renderings.

To show that this method can work in real applications, we also implement a live demo. This application consists of two parts: a hand tracker which estimates a posed MANO mesh, and a hand avatar trained using our methods on InterHand2.6M. For the pose estimator, we used the work of Zhou et al. [2020]. This method takes a stream of the monocular image from a webcam and estimates the corresponding MANO hand parameters. The estimated parameters are then used to pose and render our hand avatar at  $512 \times 334$  pixels resolution. The pose estimator takes 10 milliseconds while rendering our hand avatar takes 20 milliseconds on average, giving our system an effective speed of 33 FPS. We show the qualitative results of this demo in Fig. 5. Note the plausible high-frequency details of the rendered hand avatar driven by new poses captured live in the monocular RGB stream. We encourage the readers to check the supplementary video for the demo, as well as 3D consistent rendering sequences with view-dependent effects.

### 4.2 Comparison to State of the Art

The only other neural implicit hand model that exists in the literature is the work of [Corona et al. 2022] (LISA). As their method is trained and evaluated on an unreleased high-resolution version of the Interhand2.6M dataset and the code is not publicly available, we re-implemented their approach for a fair comparison. As an additional baseline, we use the body modeling method of [Su et al. 2021] (A-NeRF) and adapt it for hand modeling. Because our method requires a coarse hand mesh for canonicalization, we also compare against a baseline explicit method that re-textures this mesh using

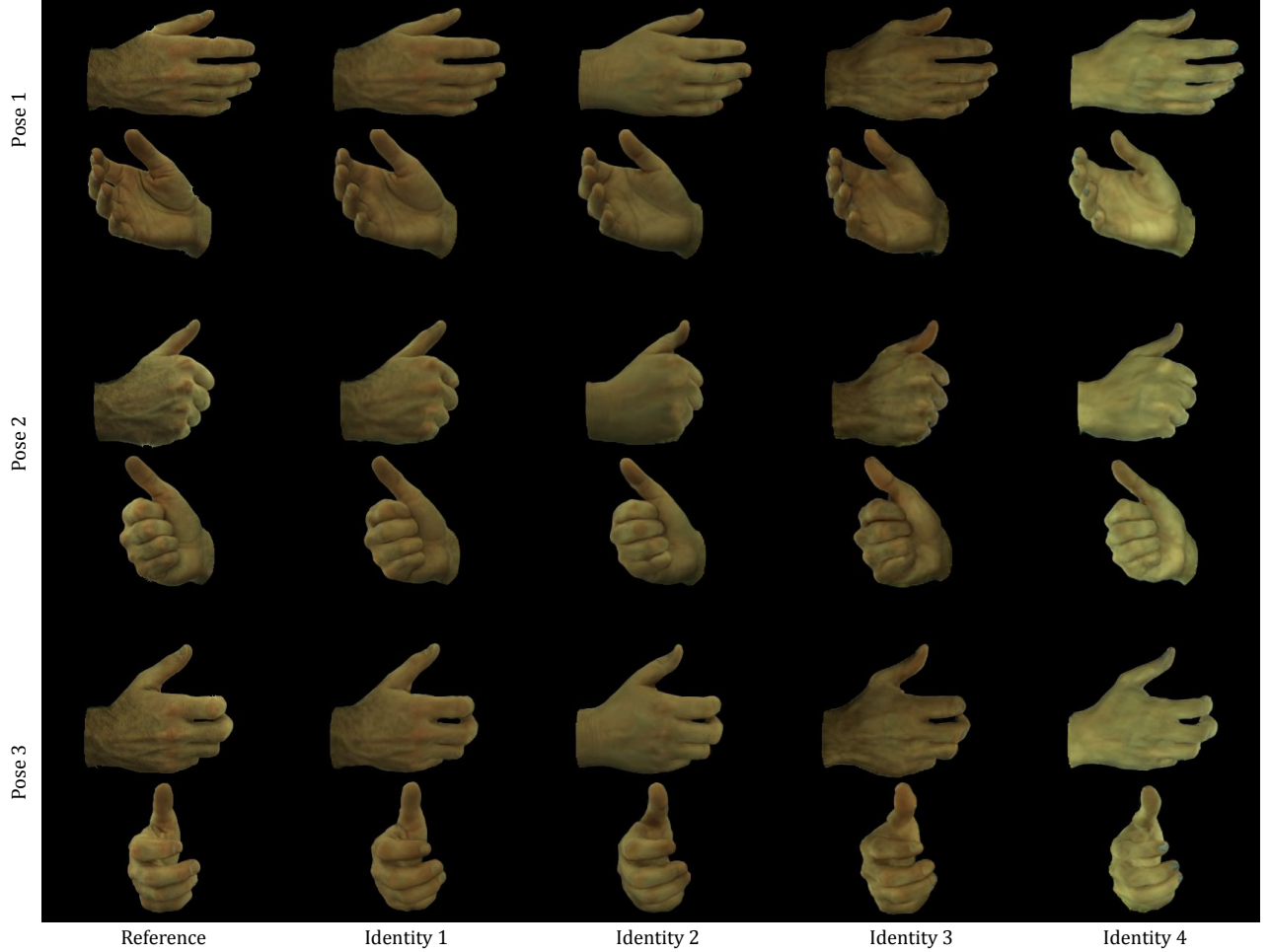


Fig. 4. **Hand Reenactment.** Our method can transfer the pose of a reference actor (Reference) to new identities (Identity 1-4). Note that our model captures pose-dependent changes, which is especially apparent for veins and in the knuckle region. It also captures view-dependent shading and self-shadowing effects.



Fig. 5. **Demo Visualization.** The demo takes in a monocular RGB input (Left) to estimate the MANO shape and pose parameters (Center). The pose is then transferred to the target identity using our method (Right).

a pre-estimated texture map (‘Mesh wrapping’). For this, we extract the texture from a flat-hand pose and wrap it to the target poses.

As shown in Table 2, our method outperforms all other neural implicit baselines while being much faster. These improvements in the metrics also translate to significant improvements in perceptual

Table 2. **Comparison on InterHand2.6M** [Moon et al. 2020b]. \* indicates we use our implementation of the approach.

	PSNR $\uparrow$	LPIPS(x1000) $\downarrow$	FID $\downarrow$	FPS $\uparrow$
Mesh wrapping	28.28	49.44	298.28	<b>82.33</b>
A-NeRF* [Su et al. 2021]	28.07	94.41	318.61	0.83
LISA* [Corona et al. 2022]	29.36	78.46	255.43	3.70
<b>Ours</b>	<b>32.04</b>	<b>25.73</b>	<b>197.39</b>	45.45

quality on the test set, which can be seen in Fig. 6. We hypothesize that this is owing to our improved canonicalization strategy and our use of perceptual loss. Both A-NeRF and LISA use per-part canonicalization similar to the one described in Eq. 3. However, learning to combine per-part output is not trivial, and could lead the ambiguities in case of severe articulations. Also as we will show in Sec. 4.3, our addition of a perceptual loss drastically improves the level of detail

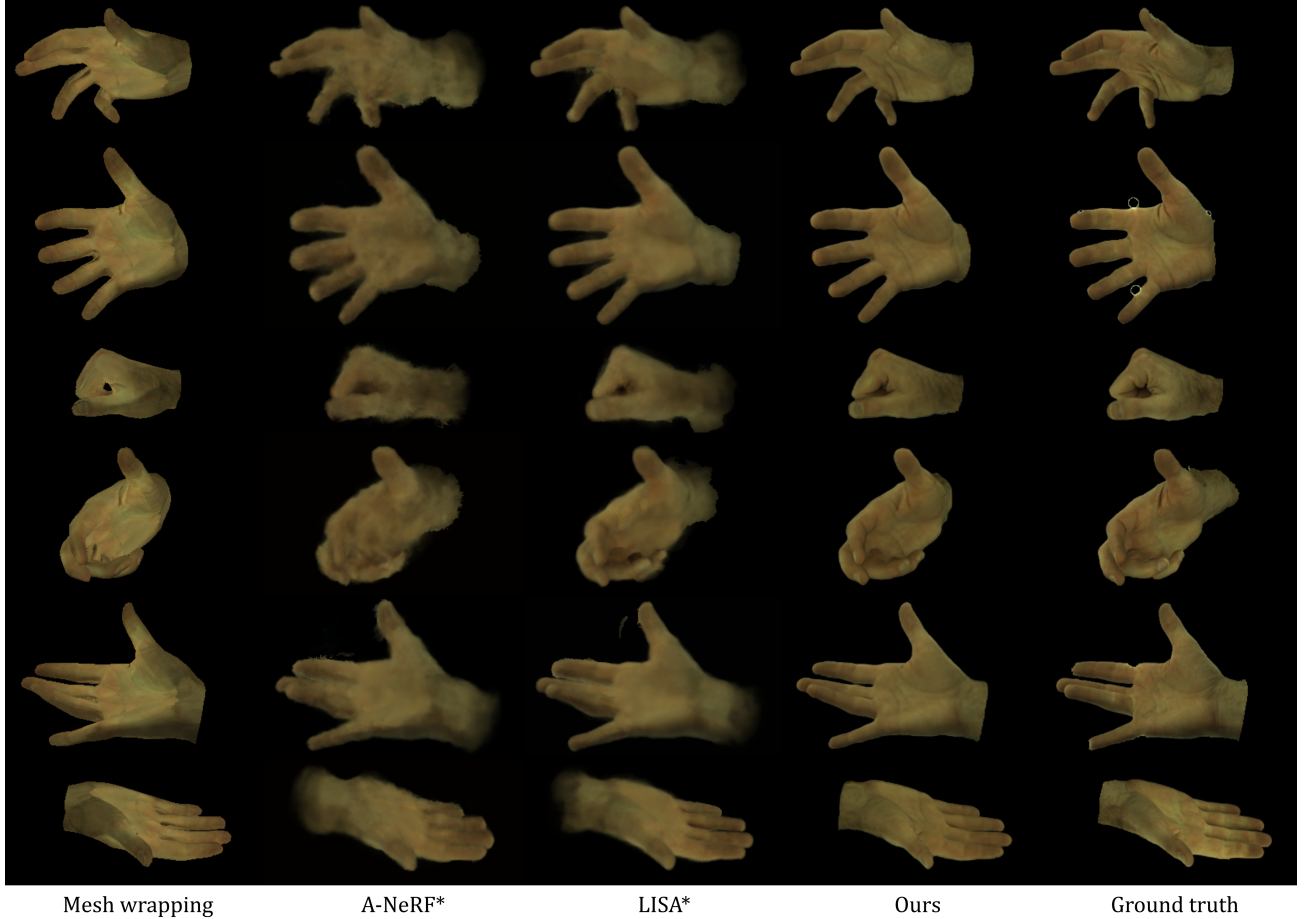


Fig. 6. **Comparison to SoTA on unseen hand poses.** A-NeRF and Mesh wrapping produce clear artifacts while LISA does not capture high-frequency details. Our method outperforms these approaches and captures high-frequency details.

the model can capture over those obtained from simple per-pixel loss used in A-NeRF and LISA.

Our method also significantly outperforms the mesh wrapping baseline, quantitatively and qualitatively. Note that modern graphics pipelines can achieve much higher frame rates for mesh rendering based on their implementation, and we only benchmark ours. But by no means can such a simple rendering achieve the complex appearance effects and photorealism as our method can. This demonstrates that our model can learn improvements upon what is possible using only the coarse geometric initialization.

### 4.3 Ablation

Our design choices are crucial for optimizing both the rendering quality and processing speed. To evaluate their significance, we performed an ablation study of various components. First, we report the impact of different canonicalization strategies on the metrics in Tab. 3 and on visual quality in Fig. 7. We see that naive pose conditioning (‘xyz’) performs the worse in all metrics, and the results are blurry and indistinct. While per-bone canonicalization (‘per-bone xyz’) produces high-quality renderings, our formulation is 1.7

Table 3. **Ablation on various canonicalization strategies.** Our approach optimizes for both quality and speed.

	PSNR $\uparrow$	LPIPS(x1000) $\downarrow$	FID $\downarrow$	#parameters $\downarrow$	FPS $\uparrow$
xyz	29.31	42.50	247.77	0.95M	43.03
per-bone xyz	<b>32.51</b>	<b>23.82</b>	198.95	1.14M	27.04
uvh w.o. pose cond.	30.33	32.36	204.24	<b>0.40M</b>	<b>45.73</b>
<b>Ours</b> (uvh w. pose cond.)	32.04	25.73	<b>197.39</b>	0.41M	45.45

times faster as it does not rely on the evaluation of multiple MLPs. Finally, our experiments show that without pose conditioning (‘uvh w.o. pose cond.’), the performance of our method drops as it is vital for capturing pose-dependent effects such as self-shadowing and skin wrinkles, and this can be seen in Fig. 7.

We evaluated the impact of mesh-guided sampling by defaulting to hierarchical sampling instead (‘w.o mesh-guided samp.’). While this produces similar rendering quality, it can be seen in Tab. 4 that our method is 5 times faster. We also evaluated the impact of the superresolution module by training our method to directly



Fig. 7. **Canonicalization Ablation.** Global xyz coordinates with naive conditioning fails to generalize to novel poses. Our proposed uvh canonicalization achieves similar visual results to per-bone xyz canonicalization while being much faster. Note that hand pose conditioning is vital for capturing pose-dependent effects such as self-shadowing (see red and green regions).

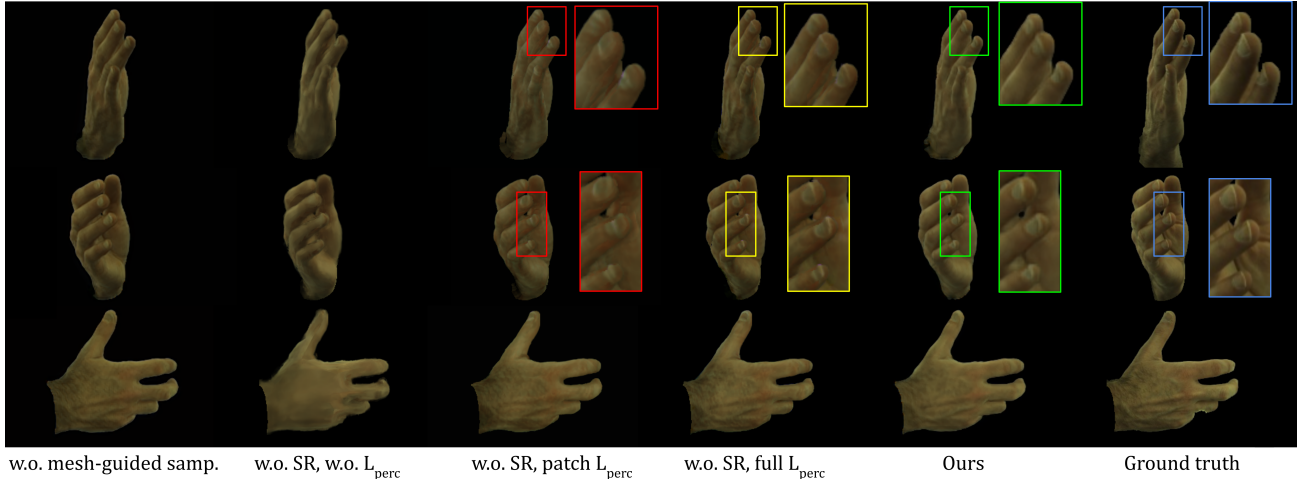


Fig. 8. **Model Ablation.** Left to right: without the mesh-guided sampling, the visual quality is good but the inference is slow (see Tab. 4); without any perceptual loss, the reconstructions lack details; with patch-based perceptual loss, subtle artifacts appear in the details (as highlighted in red); with full-image perceptual loss, these details are captured correctly (as highlighted in yellow); finally, by using a super-resolution module, the rendering speed is further improved without compromising the details (as highlighted in green).



Table 4. **Ablation study on model components.** Note that all design choices consistently improve the overall accuracy and runtime.

		PSNR $\uparrow$	LPIPS(x1000) $\downarrow$	FID $\downarrow$	FPS $\uparrow$
w.o. mesh-guided samp.		31.25	25.95	202.40	9.07
	w.o. $\mathcal{L}_{perc}$	<b>32.69</b>	38.45	226.78	19.64
w.o. SR	patch $\mathcal{L}_{perc}$	30.52	31.13	197.70	19.52
	full $\mathcal{L}_{perc}$	31.61	26.63	<b>197.35</b>	19.37
<b>Ours</b> (full $\mathcal{L}_{perc}$ )		32.04	<b>25.73</b>	197.39	<b>45.45</b>

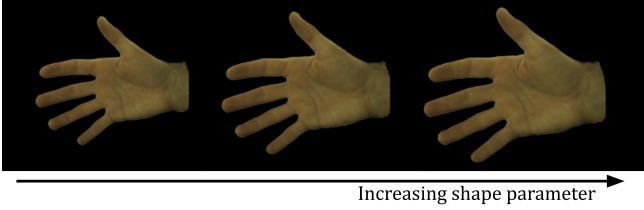


Fig. 9. Application: Shape Editing. The hand geometry can be edited without any additional retraining of the model.

render the full-resolution image instead (‘w.o. SR’). For this experiment, we investigated 3 different settings: we remove  $\mathcal{L}_{perc}$  entirely (‘w.o.  $\mathcal{L}_{perc}$ ’); we implement the commonly-used patch perceptual loss [Weng et al. 2022] where random crops of  $64 \times 64$  pixels are used for the perceptual loss instead (‘patch  $\mathcal{L}_{perc}$ ’); finally, we use the perceptual loss on the full images (‘full  $\mathcal{L}_{perc}$ ’). Tab. 4 shows that the SR module makes our method 2.4 times faster for all variants. Although the method ‘w.o.  $\mathcal{L}_{perc}$ ’ achieved the highest PSNR, adding any form of  $\mathcal{L}_{perc}$  greatly increases the level of details (see Fig. 8). This increase in realism is captured quantitatively by the lower LPIPS and FID in Tab. 4, which better reflects human preference. Furthermore, we show our novel application of the perceptual loss on the full image enabled by our efficient formulation (‘full  $\mathcal{L}_{perc}$ ’) greatly improves the rendering quality quantitatively and qualitatively. Finally, our full method (‘Ours’) achieves superior or comparable rendering quality while being significantly faster.

Overall, it is clear that our design choices optimize both rendering quality and speed, thus enabling us to photo-realistically render human hands in real-time for the first time in literature.

#### 4.4 Additional Application: Shape Editing

Our UVD encoding and the mesh-guided sampling formulation are not only advantageous in terms of rendering speed and quality, but they also enable easy editing of the hand-avatar geometry. Given the original hand parameter  $\psi_{init} : \{\theta, \beta_{init}, t, R\}$ , we can modify the shape parameter to obtain  $\psi_{new} : \{\theta, \beta_{new}, t, R\}$ . By using the corresponding mesh  $\mathcal{M}(\psi_{new})$  in the canonicalization procedure, the rendered hand appearance will change accordingly. This allows the geometry of the hand avatar to be modified without retraining. We show the results of this application in Fig. 9, where we modified the first principal component of the MANO shape parameter  $\beta$ .

## 5 DISCUSSION

### 5.1 Limitations and Future Work

While our work is an important milestone for the full digitization of human hands, there are still several avenues for future work. Since our approach depends on the MANO mesh, future work could look into improving the quality of such a mesh. This could include refining the geometry, possibly in an end-to-end manner. Another more strategic direction moving forward is to learn a generalizable implicit 3D morphable model of the human hands that is photoreal. This will give full access to all hand semantics. While our approach models hand-pose dependant illumination effects, it can not model shadow as a function of any random illumination condition other than the one the training set was captured under. We leave this modeling for future works.

### 5.2 Societal Impact

Alongside its immense applications, human modeling also presents challenging societal problems. A digital avatar of an individual has the potential of being misused by bad actors. Though detecting real vs. fake images is a possibility, a more strategic approach would be watermarking the generative models. This way, a generated image can always be attributed back to the model it was generated from. This is an active area of research, and we hope the community adopts it in their body modeling works.

## 6 CONCLUSION

We presented the first neural implicit approach that can render human hands in a photorealistic manner in real-time. Our approach is carefully designed to optimize the rendering quality and speed. At the heart of our method is a low-resolution NeRF rendering and a super-resolution module that produces 3D-consistent results. We show that a novel application of the perceptual loss on the full image space is important for generating accurate details. We also utilize the MANO hand mesh to guide the sampling of points in 3D space to better improve the rendering speed. Results show that our method generates a wide variety of hand articulations, high-frequency texture details, and pose-dependent effects. Comparison with related methods clearly shows that our approach outperforms the baselines by a significant margin. We also demonstrate editing the hand geometry while keeping the texture fixed. We hope our work encourages research into the important problem of photorealistic rendering of the human hands. For this, we will release our code.

### Acknowledgements

We thank Ashwath Shetty, Yiming Wang, Oleksandr Sotnychenko, and Basavaraj Sunagad for their help; the MPII IST department for the technical support. This work was supported by the ERC Consolidator Grant 4DRepLy (770784).

## REFERENCES

- Thiemo Alldieck, Hongyi Xu, and Cristian Sminchisescu. 2021. imghum: Implicit generative models of 3d human shape and articulated pose. In *Proceedings of the IEEE/CVF International Conference on Computer Vision*. 5461–5470.
- Timur Bagautdinov, Chenglei Wu, Tomas Simon, Fabián Prada, Takaaki Shiratori, Shih-En Wei, Weipeng Xu, Yaser Sheikh, and Jason Saragih. 2021. Driving-Signal Aware Full-Body Avatars. *ACM Trans. Graph.* 40, 4, Article 143 (jul 2021), 17 pages.

- Bharat Lal Bhatnagar, Cristian Sminchisescu, Christian Theobalt, and Gerard Pons-Moll. 2020. Combining Implicit Function Learning and Parametric Models for 3D Human Reconstruction. In *European Conference on Computer Vision (ECCV)*. Springer.
- Chen Cao, Tomas Simon, Jin Kyu Kim, Gabe Schwartz, Michael Zollhoefer, Shun-Suke Saito, Stephen Lombardi, Shih-En Wei, Danielle Belko, Shouo-I Yu, Yaser Sheikh, and Jason Saragih. 2022. Authentic Volumetric Avatars from a Phone Scan. *ACM Trans. Graph.* 41, 4, Article 163 (jul 2022), 19 pages.
- Eric R. Chan, Connor Z. Lin, Matthew A. Chan, Koki Nagano, Boxiao Pan, Shalini De Mello, Orazio Gallo, Leonidas Guibas, Jonathan Tremblay, Sameh Khamis, Tero Karras, and Gordon Wetzstein. 2022. Efficient Geometry-aware 3D Generative Adversarial Networks. In *CVPR*.
- Enric Corona, Tomas Hodan, Minh Vo, Francesc Moreno-Noguer, Chris Sweeney, Richard Newcombe, and Lingni Ma. 2022. LISA: Learning Implicit Shape and Appearance of Hands. In *Proceedings of the IEEE/CVF Conference on Computer Vision and Pattern Recognition*. 20533–20543.
- Xuan Gao, Chenglai Zhong, Jun Xiang, Yang Hong, Yudong Guo, and Juyong Zhang. 2022. Reconstructing Personalized Semantic Facial NeRF Models From Monocular Video. *ACM Transactions on Graphics (Proceedings of SIGGRAPH Asia)* 41, 6 (2022). <https://doi.org/10.1145/3550454.3555501>
- Philip-William Grassal, Malte Prizler, Titus Leistner, Carsten Rother, Matthias Nießner, and Justus Thies. 2022. Neural head avatars from monocular RGB videos. In *Proceedings of the IEEE/CVF Conference on Computer Vision and Pattern Recognition*. 18653–18664.
- Marc Habermann, Lingjie Liu, Weipeng Xu, Gerard Pons-Moll, Michael Zollhoefer, and Christian Theobalt. 2022. HDHumans: A Hybrid Approach for High-fidelity Digital Humans. *arXiv preprint arXiv:2210.12003* (2022).
- Marc Habermann, Lingjie Liu, Weipeng Xu, Michael Zollhoefer, Gerard Pons-Moll, and Christian Theobalt. 2021. Real-time Deep Dynamic Characters. *ACM Transactions on Graphics* 40, 4, Article 42 (aug 2021).
- Tao Hu, Tao Yu, Zerong Zheng, He Zhang, Yebin Liu, and Matthias Zwicker. 2021. Hvtr: Hybrid volumetric-textural rendering for human avatars. *arXiv preprint arXiv:2112.10203* (2021).
- Boyi Jiang, Yang Hong, Hujun Bao, and Juyong Zhang. 2022. SelfRecon: Self Reconstruction Your Digital Avatar from Monocular Video. In *IEEE/CVF Conference on Computer Vision and Pattern Recognition (CVPR)*.
- Korrawe Karunratanakul, Adrian Spurr, Zicong Fan, Otmar Hilliges, and Siyu Tang. 2021. A Skeleton-Driven Neural Occupancy Representation for Articulated Hands. In *International Conference on 3D Vision (3DV)*.
- Korrawe Karunratanakul, Jinlong Yang, Yan Zhang, Michael Black, Krikamol Muandet, and Siyu Tang. 2020. Grasping Field: Learning Implicit Representations for Human Grasps. In *2020 International Conference on 3D Vision (3DV 2020)*. IEEE, Piscataway, NJ, 333–344. <https://doi.org/10.1109/3DV50981.2020.00043>
- Diederik P. Kingma and Jimmy Ba. 2015. Adam: A Method for Stochastic Optimization. In *3rd International Conference on Learning Representations, ICLR 2015, San Diego, CA, USA, May 7-9, 2015, Conference Track Proceedings*, Yoshua Bengio and Yann LeCun (Eds.). <http://arxiv.org/abs/1412.6980>
- Tianye Li, Timo Bolkart, Michael J. Black, Hao Li, and Javier Romero. 2017. Learning a model of facial shape and expression from 4D scans. *ACM Transactions on Graphics, (Proc. SIGGRAPH Asia)* 36, 6 (2017), 194:1–194:17. <https://doi.org/10.1145/3130800.3130813>
- Yuwei Li, Minye Wu, Yuyao Zhang, Lan Xu, and Jingyi Yu. 2021. PIANO: A Parametric Hand Bone Model from Magnetic Resonance Imaging. In *Proceedings of the Thirtieth International Joint Conference on Artificial Intelligence, IJCAI-21*. 816–822. <https://doi.org/10.24963/ijcai.2021/113>
- Yuwei Li, Longwen Zhang, Zesong Qiu, Yingwenqi Jiang, Nianyi Li, Yuxin Ma, Yuyao Zhang, Lan Xu, and Jingyi Yu. 2022. NIMBLE: a non-rigid hand model with bones and muscles. *ACM Transactions on Graphics (TOG)* 41, 4 (2022), 1–16.
- Lingjie Liu, Marc Habermann, Viktor Rudnev, Kripasindhu Sarkar, Jiatao Gu, and Christian Theobalt. 2021. Neural Actor: Neural Free-view Synthesis of Human Actors with Pose Control. *ACM Trans. Graph. (ACM SIGGRAPH Asia)* (2021).
- Stephen Lombardi, Tomas Simon, Jason Saragih, Gabriel Schwartz, Andreas Lehrmann, and Yaser Sheikh. 2019. Neural Volumes: Learning Dynamic Renderable Volumes from Images. *ACM Trans. Graph.* 38, 4, Article 65 (July 2019), 14 pages.
- Stephen Lombardi, Tomas Simon, Gabriel Schwartz, Michael Zollhoefer, Yaser Sheikh, and Jason Saragih. 2021. Mixture of Volumetric Primitives for Efficient Neural Rendering. *ACM Trans. Graph.* 40, 4, Article 59 (jul 2021), 13 pages. <https://doi.org/10.1145/3450626.3459863>
- Haimin Luo, Teng Xu, Yuheng Jiang, Chenglin Zhou, Qiwei Qiu, Yingliang Zhang, Wei Yang, Lan Xu, and Jingyi Yu. 2022. Artemis: Articulated Neural Pets with Appearance and Motion Synthesis. *ACM Trans. Graph.* 41, 4, Article 164 (jul 2022).
- S. Ma, T. Simon, J. Saragih, D. Wang, Y. Li, F. La Torre, and Y. Sheikh. 2021. Pixel Codec Avatars. In *2021 IEEE/CVF Conference on Computer Vision and Pattern Recognition (CVPR)*. 64–73.
- Ben Mildenhall, Pratul P. Srinivasan, Matthew Tancik, Jonathan T. Barron, Ravi Ramamoorthi, and Ren Ng. 2020. NeRF: Representing Scenes as Neural Radiance Fields for View Synthesis. In *ECCV*.
- Gyeongseok Moon, Takaaki Shiratori, and Kyoung Mu Lee. 2020a. DeepHandMesh: A weakly-supervised deep encoder-decoder framework for high-fidelity hand mesh modeling. In *European Conference on Computer Vision*. Springer, 440–455.
- Gyeongseok Moon, Shouo-I Yu, He Wen, Takaaki Shiratori, and Kyoung Mu Lee. 2020b. InterHand2.6M: A Dataset and Baseline for 3D Interacting Hand Pose Estimation from a Single RGB Image. In *European Conference on Computer Vision (ECCV)*.
- Atsuhiko Noguchi, Xiao Sun, Stephen Lin, and Tatsuya Harada. 2021. Neural Articulated Radiance Field. In *International Conference on Computer Vision*.
- Georgios Pavlakos, Vasileios Choutas, Nima Ghorbani, Timo Bolkart, Ahmed A. A. Osman, Dimitrios Tzionas, and Michael J. Black. 2019. Expressive Body Capture: 3D Hands, Face, and Body from a Single Image. In *Proceedings IEEE Conf. on Computer Vision and Pattern Recognition (CVPR)*. 10975–10985.
- Sida Peng, Junting Dong, Qianqian Wang, Shangzhan Zhang, Qing Shuai, Xiaowei Zhou, and Hujun Bao. 2021a. Animatable neural radiance fields for modeling dynamic human bodies. In *Proceedings of the IEEE/CVF International Conference on Computer Vision*. 14314–14323.
- Sida Peng, Yuanqing Zhang, Yinghao Xu, Qianqian Wang, Qing Shuai, Hujun Bao, and Xiaowei Zhou. 2021b. Neural body: Implicit neural representations with structured latent codes for novel view synthesis of dynamic humans. In *Proceedings of the IEEE/CVF Conference on Computer Vision and Pattern Recognition*. 9054–9063.
- Sergey Prokudin, Michael J Black, and Javier Romero. 2021. SMPLpx: Neural Avatars from 3D Human Models. In *Proceedings of the IEEE/CVF Winter Conference on Applications of Computer Vision*. 1810–1819.
- Neng Qian, Jiayi Wang, Franziska Mueller, Florian Bernard, Vladislav Golyanik, and Christian Theobalt. 2020. HtM: A parametric hand texture model for 3d hand reconstruction and personalization. In *European Conference on Computer Vision, (ECCV)*. Springer, 54–71.
- Amit Raj, Julian Tanke, James Hays, Minh Vo, Carsten Stoll, and Christoph Lassner. 2021. Anr: Articulated neural rendering for virtual avatars. In *Proceedings of the IEEE/CVF Conference on Computer Vision and Pattern Recognition*. 3722–3731.
- Edoardo Remelli, Timur Bagautdinov, Shunsuke Saito, Chenglei Wu, Tomas Simon, Shih-En Wei, Kaiwen Guo, Zhe Cao, Fabian Prada, Jason Saragih, and Yaser Sheikh. 2022. Drivable Volumetric Avatars Using Texel-Aligned Features. In *ACM SIGGRAPH 2022 Conference Proceedings (Vancouver, BC, Canada) (SIGGRAPH '22)*. Association for Computing Machinery, New York, NY, USA, Article 56, 9 pages.
- Javier Romero, Dimitrios Tzionas, and Michael J. Black. 2017. Embodied Hands: Modeling and Capturing Hands and Bodies Together. *ACM Transactions on Graphics, (Proc. SIGGRAPH Asia)* 36, 6 (Nov. 2017), 245:1–245:17. <https://doi.org/10.1145/3130800.3130883>
- Ruizhi Shao, Liliang Chen, Zerong Zheng, Hongwen Zhang, Yuxiang Zhang, Han Huang, Yandong Guo, and Yebin Liu. 2022. FloRen: Real-time High-quality Human Performance Rendering via Appearance Flow Using Sparse RGB Cameras. In *SIGGRAPH Asia Conference Papers*.
- Karen Simonyan and Andrew Zisserman. 2014. Very deep convolutional networks for large-scale image recognition. *arXiv preprint arXiv:1409.1556* (2014).
- Shih-Yu Su, Frank Yu, Michael Zollhoefer, and Helge Rhodin. 2021. A-nerf: Articulated neural radiance fields for learning human shape, appearance, and pose. *Advances in Neural Information Processing Systems* 34 (2021), 12278–12291.
- Xin Suo, Yuheng Jiang, Pei Lin, Yingliang Zhang, Minye Wu, Kaiwen Guo, and Lan Xu. 2021. NeuralHumanFV: Real-Time Neural Volumetric Human Performance Rendering using RGB Cameras. In *2021 IEEE/CVF Conference on Computer Vision and Pattern Recognition (CVPR)*. 6222–6233. <https://doi.org/10.1109/CVPR46437.2021.00616>
- Chung-Yi Weng, Brian Curless, Pratul P. Srinivasan, Jonathan T. Barron, and Ira Kemelmacher-Shlizerman. 2022. HumanNeRF: Free-Viewpoint Rendering of Moving People from Monocular Video. In *Proceedings of the IEEE/CVF Conference on Computer Vision and Pattern Recognition (CVPR)*. 16210–16220.
- Feng Xu, Yebin Liu, Carsten Stoll, James Tompkin, Gaurav Bharaj, Qionghai Dai, Hans-Peter Seidel, Jan Kautz, and Christian Theobalt. 2011. Video-based Characters – Creating New Human Performances from a Multi-View Video Database. *ACM Transactions on Graphics* 30 (07 2011), 32. <https://doi.org/10.1145/2010324.1964927>
- Gengshan Yang, Minh Vo, Natalia Neverova, Deva Ramanan, Andrea Vedaldi, and Hanbyul Joo. 2022. Banmo: Building animatable 3d neural models from many casual videos. In *Proceedings of the IEEE/CVF Conference on Computer Vision and Pattern Recognition*. 2863–2873.
- Richard Zhang, Phillip Isola, Alexei A. Efros, Eli Shechtman, and Oliver Wang. 2018. The Unreasonable Effectiveness of Deep Features as a Perceptual Metric. In *Proceedings of the IEEE Conference on Computer Vision and Pattern Recognition (CVPR)*.
- Yufeng Zheng, Victoria Fernández Abrevaya, Marcel C. Bühler, Xu Chen, Michael J. Black, and Otmar Hilliges. 2022. I M Avatar: Implicit Morphable Head Avatars from Videos. In *IEEE/CVF Conf. on Computer Vision and Pattern Recognition (CVPR)*. 13545–13555.
- Yuxiao Zhou, Marc Habermann, Weipeng Xu, Ikhsanul Habibie, Christian Theobalt, and Feng Xu. 2020. Monocular Real-Time Hand Shape and Motion Capture Using Multi-Modal Data. In *IEEE/CVF Conference on Computer Vision and Pattern Recognition (CVPR)*.